

Critical Infrastructure Resilience of the Distribution Grid

Faculty Investigators:

UNCC: Dr. Badrul Chowdhury, Dr. Asis Nasipuri, Dr. Churlzu Lim, and Dr. K.R. Subramanian

Clemson: Dr. Elham Makram, Dr. Hany Abdel-Salam

Student Investigators:

UNCC; Krupa Mahesh, Darshan Prabhu, Md. Shakawat Hossan, Mohit Arora, Chris Grafer

Clemson: Shane Kimble

SUMMARY

Hurricanes, ice storms, tornadoes, and other significant high-impact, low frequency (HILF) weather events have been known to cause massive disruptions in power leading to significant customer miseries in the recent past. The main goal of this project is to develop optimal reconfiguration and constrained resource distribution to maximize the availability of power to critical loads based on intelligence gathered from a wireless sensor network (WSN) during HILF events. The grid resiliency improvement solution features extensive use of distributed energy resources (DER) as well as the emerging concept of a microgrid operating within a WSN for enhanced responsiveness and faster restoration of power to critical loads (such as, healthcare facilities, law enforcement, natural gas delivery network, gasoline pumping stations, water distribution facilities, etc.). A multi-tiered wireless sensor network is designed that has the ability to report to the substation with information on the attributes of an outage, including location, possible extent of the outage, and potential use of DER for backup power. The sensors used in this system are Rogowski coils and tilt sensors along with MicaZ sensor motes. The solution, called *Reconfiguration, Optimization And Mobilization of Energy Resources* (ROAMER) will eventually have the capability for massive mobilization of DER through reconfiguration of power lines and mobile backup power generation (residential/commercial rooftop and community solar plants, plug-in electric vehicles (PEV), and portable diesel generators) in order to provide power to critical loads, such as healthcare network, natural gas delivery network, gasoline pumping stations, water distribution facilities, etc.

1. INTRODUCTION

The resilience of any infrastructure hinges on its ability to anticipate, absorb, and/or rapidly recover from a disruptive event. The power distribution infrastructure is inherently vulnerable to outages considering the fact that thousands of miles of critical current-carrying wires are exposed to the elements. This fact coupled with the realities of an aging infrastructure and continuously changing operating dynamics and constraints render the power grid fully exposed to the vagaries of nature. The objective of this project is to improve the power distribution network resiliency, thereby decreasing the power grid recovery time. This project targets the recovery aspect of resiliency. Modern networked data sensing and processing technologies offer unlimited potential for multimodal sensing, distributed processing, and dynamic adaptability to changing conditions. In particular, wireless sensor networking technologies can enable the development of systems that enhance the speed and accuracy of detecting emergency events and perform distributed computing to optimally deploy mobile power sources; reconfigure nearby available DERs to energize critical loads; and identify healthy power lines through which to deliver power from rooftop solar and community energy storage devices to critical loads. The key challenge is to quickly and efficiently solve this mobilization and reconfiguration problem using a diverse set of inputs. The proposed research presents a unified approach for designing the system architecture to handle such computation and communication intensive operations, as well as developing appropriate algorithms for automated hazard detection and generation of valid reconfiguration.

To explain how our system works in a nutshell - imagine a system consisting of three tiers. The first tier comprises of the sensor network. Our intent is to detect the stability of the power poles, i.e. to check if any pole is tilted more than what is considered to be safe for the functioning of the power grid. Along with this, we also intend to detect and measure the current flowing in the power lines to check if there is any abnormality in the current flow or detect an outage in the grid. These sensors are connected to data acquisition boards which communicate wirelessly with tier two consisting of ZigBee modules. These modules constitute the wireless communication devices that collect data coming from tier I (sensor motes) and send it to Tier III. Tier III includes the communication tower and the visualization system which reflects the health of the power grid and updates periodically. Our aim is to make this a low cost, efficient system.

2. RELATED WORK

Extensive research was done before deciding what sensors to use in our project. It was found that current transformers are the most commonly used line sensors. Tollgrades' [9] MV sensors use inductive powering and use wireless communication protocols like Wi-Fi or the cellular network. They can measure the RMS current, fault and surge currents. They have a wide range of working, however they are bulky and expensive while compared to the solution proposed in our system.

Another solution found was to make use of optical current and voltage sensor [10]. This was a very interesting method to sense current and voltage. The paper talks about using a hollow core composite silicone polymer insulator to support a high voltage conductor. It makes use of optical fiber which carries digitized current and voltage data from the MetPod to an interface module. It works as follows: A collimated light source located at the high voltage end is circularly polarized before passing through an aperture. The optical beam then passes through one or more optical crystals located along the length of the hollow core insulator. Electro-optic crystal modulates the state of polarization of the light in direct proportion to the voltage drop across that crystal. However, these sensors are very bulky and very expensive.

Several other papers show the usage of CTs for current measurement like Cooper power systems by Eaton [11], Schneider Electric [13] and so on. However these have their own disadvantages which can be overcome by using a different sensor.

Hall sensors are small, low cost sensors which can be used to measure very high currents [15]. It has its own drawbacks – the output from Hall Effect sensor has a large temperature drift and usually requires a stable external current source. Giant magneto resistors The GMR current sensor shows excellent performance and is cost effective, making it suitable for applications such as steady-state and transient-state monitoring [8]. With the advantages of having a high sensitivity, high linearity, small volume, low cost, and simple structure, the GMR current sensor is promising for the measurement and monitoring of smart grids, except for its temperature drift as in the case of Hall sensors. Also the drift can go up to 0.3% which is high when compared to Rogowski Coil.

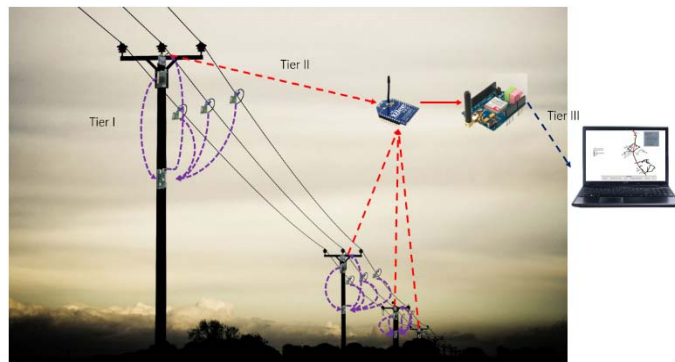


Figure 1. The proposed WSN

For comparison, sensor characteristics are compared and tabulated in Table I.

TABLE I. VARIOUS CURRENT SENSORS

Sensors	Optical Current Sensors	Fluxgate	Shunt	FOCT
Volume	Bulky	Bulky	Small	Small
Cost	High	High	Low	Extra High
Voltage Range	< 37kV	--	< 4kV	< 1600kV
Current Range	200A ~ 10kA	1A ~ 10kA	mA ~ kA	< 600kA
Accuracy	0.3%	0.5%	0.5%	0.5%
Temperature Range	-20°C to +60°C	-50°C to +80°C	-40°C to +125°C	--
Ease of Installation	Clamp On	Medium	Complex	Medium
Sensors	Hall Sensor	GMR	CT	Rogowski Coils
Volume	Small	Small	Bulky	Small
Cost	Low	Low	High	Low
Voltage Range	--	--	< 25 kV	7.5kV - 500kV
Current Range	10mA ~ 35kA	1mA ~ 10kA	1A ~ 100kA	< 400kA
Accuracy	0.2%	0.3%	0.4-0.5%	0.15%
Temperature Range	-40°C to +150°C	-40°C to +150°C	--	-40°C to +150°C
Ease of Installation	Medium	Clamp On	Clamp On	Easy (Clamp On)

3. THE PROPOSED SYSTEM

Our objective is to sense the current in the power lines and the angle of tilt in the power poles. Two kinds of sensors are used for this purpose: Rogowski coil and Tilt sensor respectively. The sensors collect data and send them to the wireless communication modules. This data is then sent to the visualization system where it is updated. If there is any abnormal functioning of the power grid, the visualization system shows alerts using color codes. The optimization system then makes use of this data and optimizes the way DERs and PVs can be used to power up critical nodes. To break this down, we use a three tier system as explained below.

The proposed system is shown in Figure 1. The three tiers are as follows: tier I includes a tilt sensor attached onto the top of each of the poles, Rogowski coil sensors on power lines that are intended to be monitored, and a ZigBee PRO module on each pole.

Tier I wireless communication comprises of the data collected from each of the sensors and passed on to the ZigBee PRO module on their respective poles (ZigBee End-device). The tilt sensor measures the angle of tilt of the pole it is attached to. If a pole tilts more than what can be considered safe or until the power line almost snaps, then the sensor alerts the substation with the help of the visualization system. Tier I communication steps are shown in Figures 2, 3 and 4.

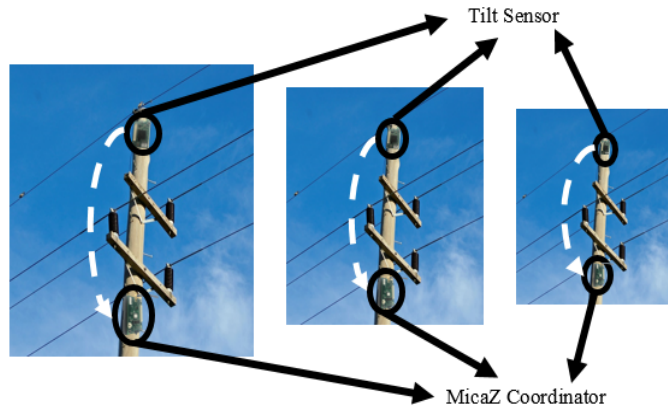


Figure 2. Tier I Communication

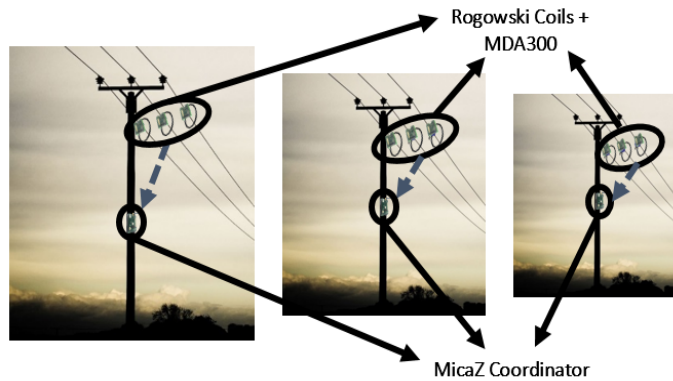


Figure 3. Tier I Communication

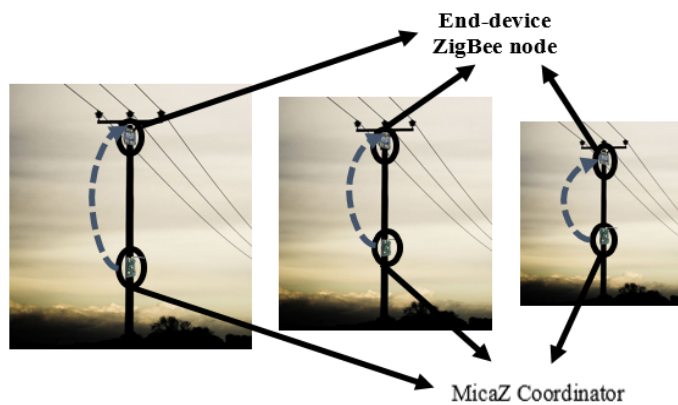


Figure 4. Tier I Communication

Tier II consists of the communication between the ZigBee end- devices that are attached onto poles and the ZigBee PRO device that acts as a ZigBee Coordinator. Whatever sensor data the end-device gets, is passed to the coordinator module. This module is attached to a GSM module. Tier II communication is shown in Figure 5.

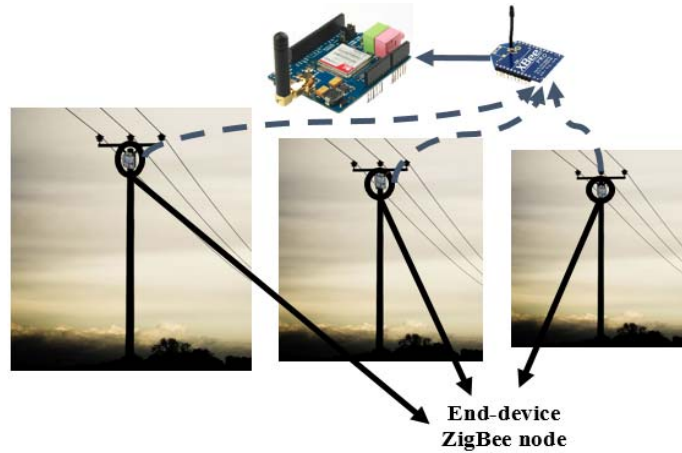


Figure 5. Tier II Communication

Tier III is the communication between the GSM module and the GSM tower and network. 3G and HTTP together help us send sensor data wirelessly to the visualization software and update periodically. The multi-tiered wireless network is designed for robustness and resiliency for efficiently transmitting the sensor information to the substation for appropriate reconfigurations during disruptive events. Tier III communication is shown in Figure 6.

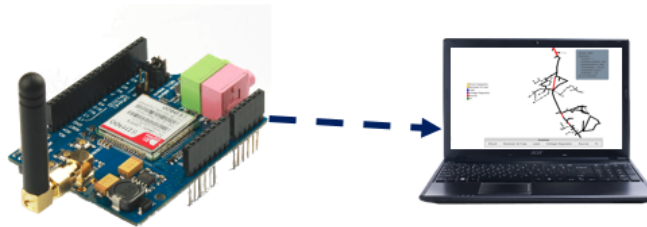


Figure 6. Tier III Communication

The wireless communication network, visualization system and optimization system that were developed by my colleagues are discussed in this section. The development of sensors is discussed in detail in the next section.

A. Wireless Communication Network

Once all the sensor data is collected from the Rogowski coils and Tilt sensors, the MicaZ coordinators on each pole forward the data to an XBee Pro Module located on respective poles. These are considered to be end-device XBee Pro modules. The XBee Pro Modules meet IEEE 802.15.4 communication protocol and support the unique needs of low-cost, low-power wireless sensor networks. They provide reliable delivery of data between devices. The modules operate within the ISM 2.4 GHz frequency band. The outdoor range of XBee Pro is up to 2 miles (line of sight) and indoor range up to 90 meters.

This communication is also a part of tier I as shown in Figure 4. The ZigBee end-device then forwards the data to the ZigBee Coordinator node, which is also a ZigBee Pro module. The only difference is that a

SIM900 GSM module is attached on to the coordinator node. This module helps in sending the data fast and effortlessly using HTTP which is tier II (Figure 5).

The SIM900 GSM module is a quad band GSM/GPRS module that works on 850MHz, EGSM 900MHz, DCS 1800 MHz and PCS 1900MHz. The frequency bands can be set using AT commands. The current consumption is as low as 1.0 mA in sleep mode. The GSM module is interfaced with Arduino UNO microcontroller. The software used to program these modules is the Arduino IDE.

B. Visualization System

The data from the ZigBee Coordinator is received by the GSM module and then uploaded to the mongo server. The visualization system uses the MAMP server for this application. Using the data uploaded to the server, the visualization software updates its status and shows the values of current and inclination of poles when hovered over the nodes. If there is a significant drop or spike in current or an inclination of more than a particular angle value, the node turns red to indicate that there is a fault in that node.

C. Optimization System

A mathematical programming approach is used to optimally dispatch available DERs when power outage occurs due to stormy weather. In particular, the problem is formulated as a mixed integer linear program (MILP). We assume that nodes can be classified into three types, DER node, regular node, and critical node. A DER node represents the location where a DER is installed. Both regular and critical nodes are loads, but critical nodes are considered to have higher priority to regular nodes. The goal of the DER dispatch problem is to identify load nodes that are supplied from DERs.

In case there is any fault in the grid and the sensors send alerts through the visualization system, the information about faulty lines and available DERs is delivered to the optimization module, which solves the following optimization problem: a mixed-integer model lets the available DERs pick up critical loads during an outage. The objective here is to maximize the total sum of priority scores, which are assigned to loads in the outage-affected network using the relative importance (e.g., critical vs. non-critical loads). The set of constraints includes the set partitioning requirements, capacities of DERs, precedence of connectivity, power flow balance and voltage loss constraints.

4. VISUALIZATION SOFTWARE DEVELOPMENT

For this phase of the project, The main goal was to build a visualization tool to implemente the Duke Energy Kudzu Network feeder system shown in Figure 7.

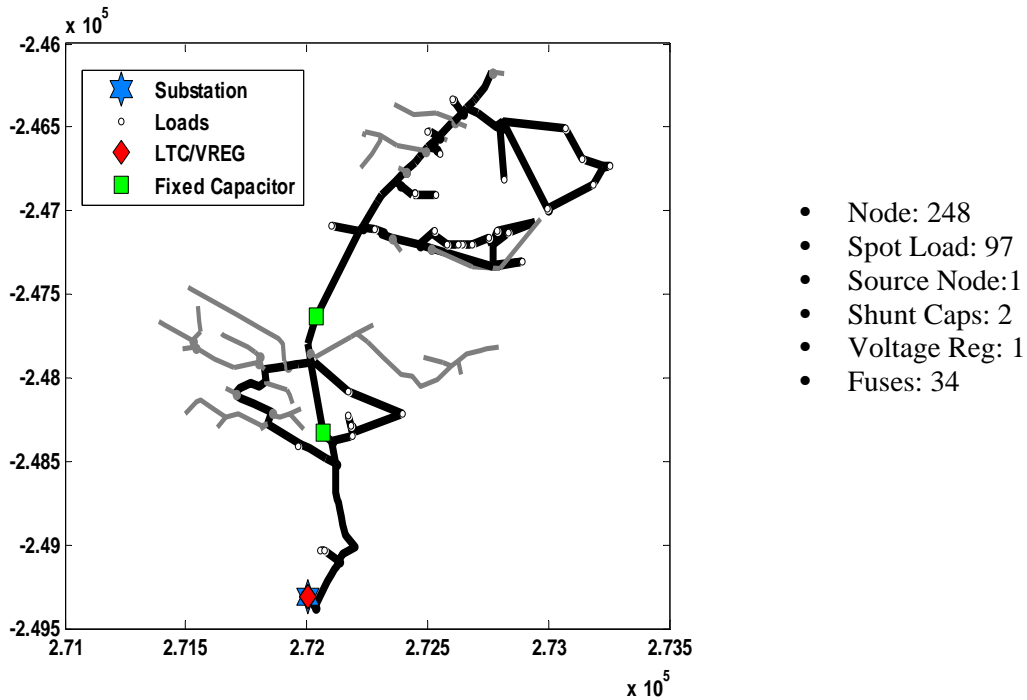


Figure 7. Duke Kudzu Network

A. Simulation Tools

Visualization software is consisted of Java program that actually pulls the data from GIS map. The retrieved data is sent to the Mongo database which is a cross platform document oriented cloud database. There is one additional JavaScript program which has a bidirectional flow with MongoDB to receive the data and acknowledge (See Fig. 8).

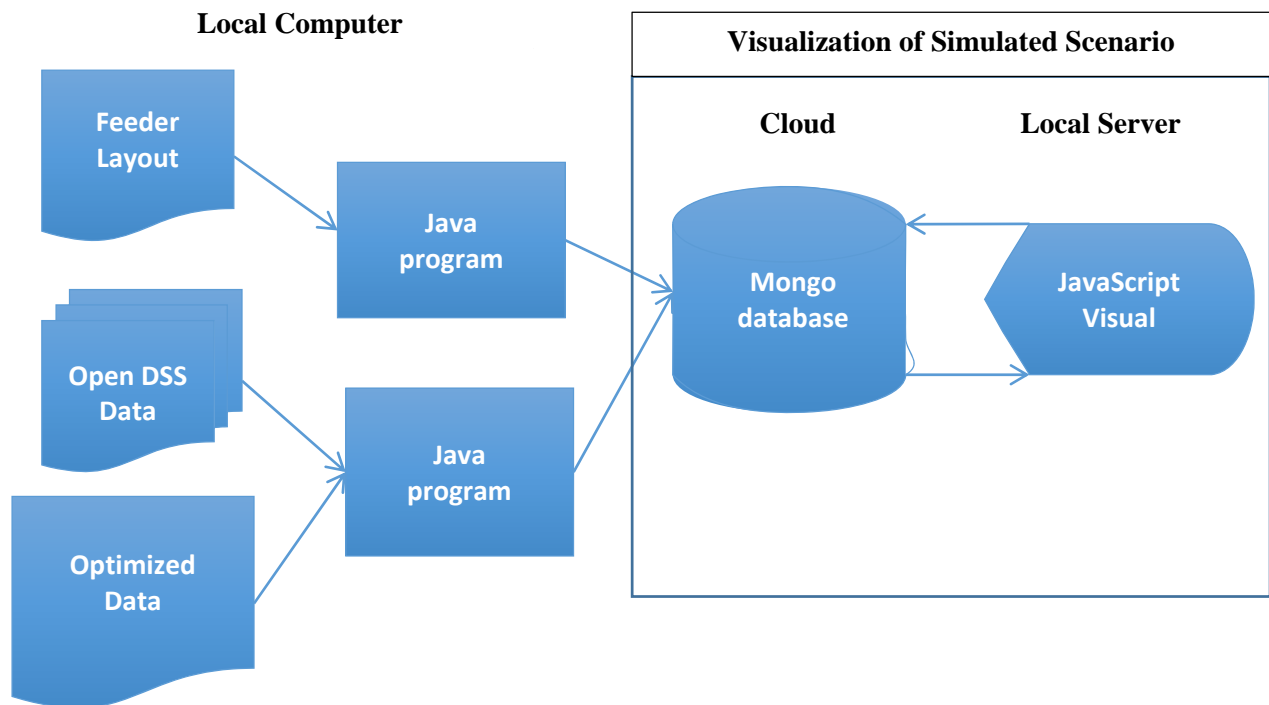


Figure 8. Visualization software construction

B. Simulated Feeder

The simulated feeder system, obtained from the project sponsor, is shown again in Figure 9, but this time with the possible location of distributed PV. To create the fault in the system recloser-fuse coordination was used. Visualization software was able to receive the whole system data including DERs. Feeder with DER placement and coordinated recloser-fuse locations are shown as following figures.

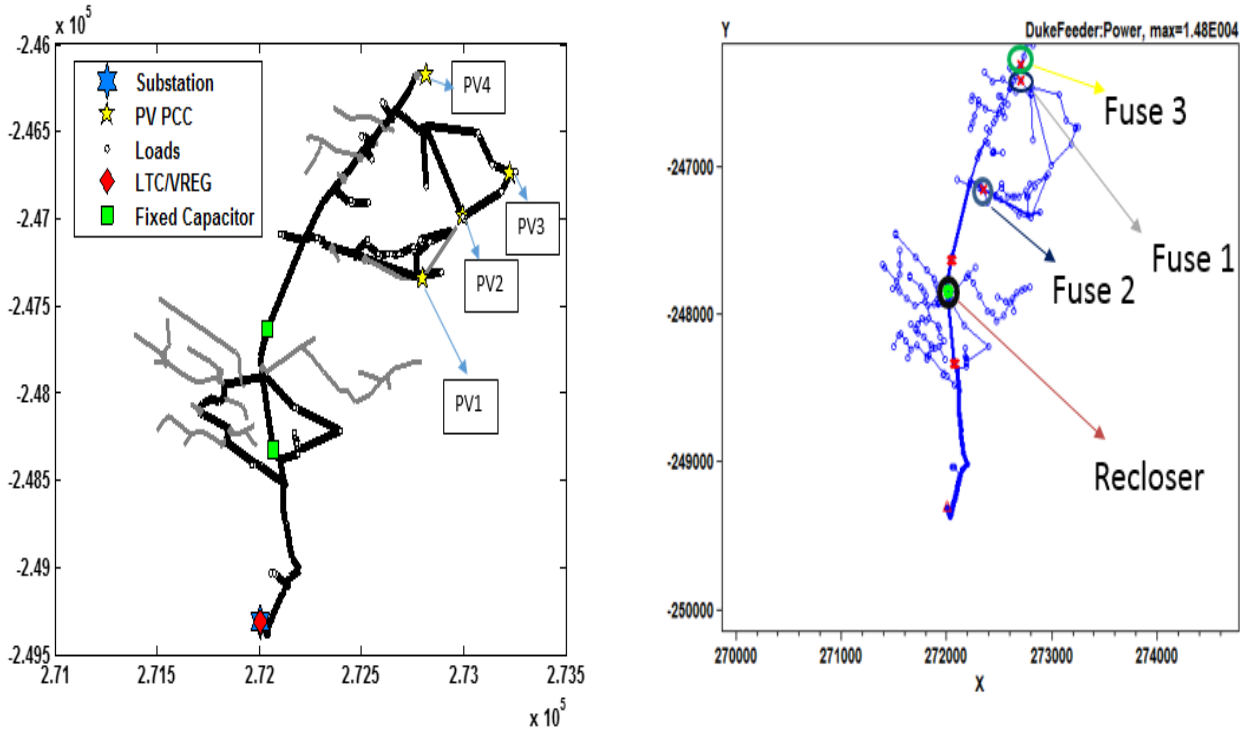


Figure 9: a) Feeder with PV integration, b) Recloser coordination with fuse 1, 2 & 3

5. SENSOR DEVELOPMENT

We now present the design and development of the sensors, which is the main focus of this report. Finding sensors for this application is critical and needs careful planning. The sensors chosen must meet these requirements:

- High efficiency
- High accuracy
- High reliability
- Low cost
- Easy to install
- Less bulky
- Immune to environmental changes
- Low maintenance

- Better than what is used now.

Even after checking these points off our list, there were a few challenges. How would the components be powered? Can they be powered inductively or using small solar panels? If they are powered inductively, how to keep the sensors running for a while even when the power line is down? How and where to efficiently place the sensors on poles? Do any of these components need maintenance? If so, how often and what is the cost estimate of this maintenance? These are just some of the questions that need to be thought about and overcome while building our system.

After extensive research in the area, two sensors were chosen to be used in this system: MicaZ sensor motes with accelerometer for tilt sensor, Rogowski coils for current sensing. These sensors are explained in detail below.

A. Tilt Sensor

This sensor is developed to measure the tilt of a pole when it is attached onto it. MicaZ sensor motes interfaced with MTS300CA sensor boards are used to implement the tilt sensor. These components are shown in Figures 6 and 7. MIB510 programmer board is used to program the MicaZ motes (shown in Figure 8).



Figure 6. MicaZ Mote



Figure 7. MTS300CA Sensorboard



Figure 8. MIB510 Programmer

MicaZ motes are modules that are used in low-power wireless sensor networks. They work at 2.4 GHz frequency and are IEEE 802.15.4 compliant. They have a data rate of 250 kbps. The MTS300CA is a sensor board with a variety of sensing modules. These sensors can be used in a wide range of applications like clap activated light system, movement sensing, robotics, and other applications. We make use of the ADXL202JE MEMS 2-axis accelerometer to implement the tilt sensor. TinyOS is used, and the NesC program is uploaded onto the MicaZ mote that will be used as the tilt sensor, using the MIB510 programmer.

Each mote is programmed such that when it is attached to a pole and is turned on, it takes the first reading as its default reading in terms of degrees. Once it is installed, it takes periodic readings of the tilt angles and updates the substation through the visualization system. In case of any disruption, if the pole tilts more than a particular angle, it alerts the system. This accelerometer gives reading in terms of hexadecimal values which are then converted to decimal values and then to degrees. The tilt sensor takes readings every few seconds, minutes or hours as required.

Two kinds of sensor motes are used in this implementation: the end-device motes and the coordinator motes. The end-device motes are interfaced with an MTS300CA sensorboard each. These devices are attached on

power poles and collect data from the sensorboard and send it to their coordinator sensor motes respectively. The coordinator sensor mote is not connected to an MTS300CA sensorboard.

The end-device motes are programmed with an application that lets us visualize sensor readings on the PC. We make use of the accelerometer which gives its readings to the 10 bit ADC in the sensorboard. The sensor application periodically samples the accelerometer sensor and broadcasts the data over its radio. Each mote is given a node ID to distinguish between the data sent and to easily locate them on the visualization system. The coordinator mote is programmed with the coordinator MLME program. This program is a simple bridge between the active messages over the radio and the serial links.

The data received from the ADC is then processed to find the angle of inclination of the pole in terms of degrees. First the data is converted from hex to decimal format and then the angles are calculated from these decimal values. As soon as the motes are turned on, the first reading that the end-device motes take are made to be the default readings. Whatever readings are taken after this are compared to this default reading and the difference in angle is calculated and updated. When the difference in angle in any mote is more than a particular value, the visualization system shows the particular node to be flashing red, and thus alerting the substation that the pole is down or dangerously tilted. The node ID is displayed along with this so as to narrow down the location to that particular mote. This implementation makes the system efficient, since the affected pole can be pointed out without much delay/discrepancy.

B. Advantages of using MTS300CA as a Tilt Sensor

The MTS300CA sensorboard has a 10 bit ADC, so we get a good resolution. It also has good sensitivity and accuracy. The MicaZ motes are battery powered. They run on voltages from 3.6V to 2.7V. The table below shows how power efficient the motes are.

TABLE II. CURRENT REQUIREMENTS FOR MOTES

Operating Current (mA)	MICAz
ATMega128L, full operation	12 (7.37 MHz)
ATMega128L, sleep	0.010
Radio, receive	19.7
Radio, transmit (1 mW power)	17
Radio, sleep	0.001

The consumption of battery power is very low as shown above, especially in sleep modes. Thus, as shown in Table III, the motes can last up to a few months without needing a change/recharging of batteries. The RF transmission power can be changed as needed, anywhere between 0 dBm (1mW) and -25 dBm. Lower power can be used when interference is to be avoided, while higher power can be used when we require the motes to transmit long distance.

TABLE III. ESTIMATE OF BATTERY LIFE FOR MOTES

SYSTEM SPECIFICATIONS		
Currents		Example Duty Cycle
Processor		
Current (full operation)	8 mA	1
Current sleep	8 μ A	99
Radio		
Current in receive	8 mA	0.75
Current transmit	12 mA	0.25
Current sleep	2 μ A	99
Logger Memory		
Write	15 mA	0
Read	4 mA	0
Sleep	2 μ A	100
Sensor Board		
Current (full operation)	5 mA	1
Current sleep	5 μ A	99
Computed mA-hr used each hour		
Processor		0.0879
Radio		0.0920
Logger Memory		0.0020
Sensor Board		0.0550
Total current (mA-hr) used		0.2369
Computed battery life vs. battery size		
Battery Capacity (mA-hr)		Battery Life (months)
250		1.45
1000		5.78
3000		17.35

The radio power consumption is 17.5 mA at full power and 8.5 mA at lowest power. Screenshots of the working of this system is shown below for better understanding.

C. Observations and Results

```

Xbee sent
...
X Angle: 99
Y Angle: 0
...
Xbee sent

GSM Shield testing.
status=READY
status=ATTACHED
Node Id 5
Value in X Direction : 97
Value in Y Direction : 0
message type:
Number of data received:
49
Data received:
HTTP/1.1 200 OK
Content-Type: text/html; charset
-
    
```

Figure 9. Reading on ZigBee end-device, reading on ZigBee coordinator

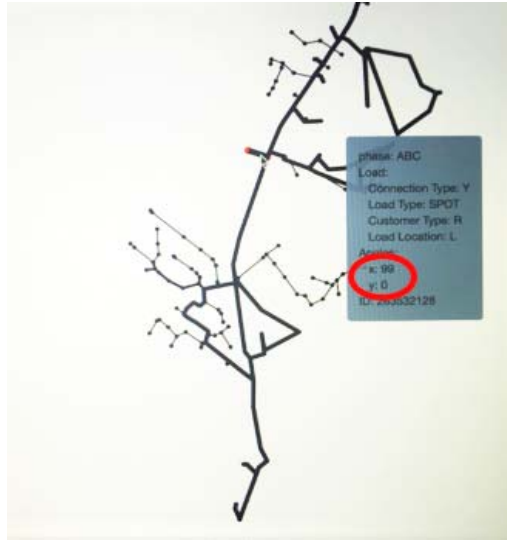


Figure 10. Values reflected on the visualization system

Figure 9 shows the x and y axes tilt values in degrees in the position that is set as the default position of the tilt sensor on the ZigBee end-device. The same values are reflected on the ZigBee coordinator. Once these values are updated on the visualization system, if that particular node is hovered over, a window pops up showing the x and y axes values (Figure 10).

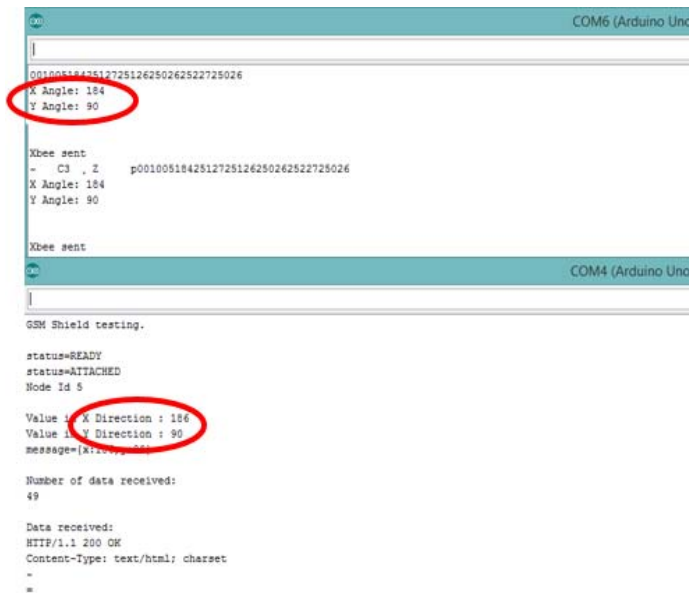


Figure 11. Reading on ZigBee end-device, reading on ZigBee coordinator

When the position of the tilt sensor is changed, the x and y axes tilt values in degrees are updated on the ZigBee end-device (Figure 11). The same values are reflected on the ZigBee coordinator.

The visualization system updates its values and reflects the same. Since the default value is set as 99 degrees in the x-axis and 0 degrees in the y-axis and is programmed such that a change of more than 45 degrees in any axis will send out alerts to the substation through the visualization system. Thus that particular node goes

red when the values 186 in the x-axis and 90 degrees in the y-axis are updated on the system, as shown in Figure 12.

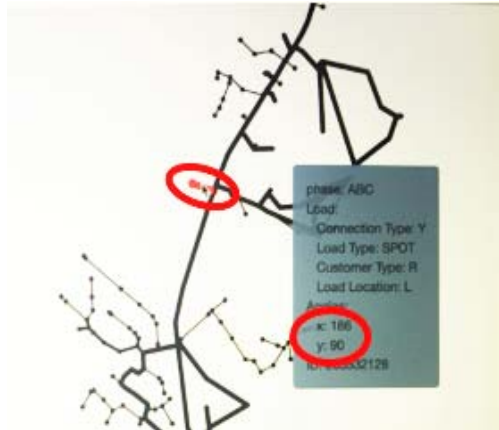


Figure 12. Values reflected on visualization system

D. Line Current Sensor

This sensor is developed with the intention of detecting and measuring the current in the power line that it is clamped around. Rogowski coils (RCs) are very similar to conventional current transformers except a few changes that improve its performance. One of the main change is that the Rogowski coil has an air core while compared to the iron core in CTs. The Rogowski coil is made of wire loop winding just like CTs, except that the end of the wire loop is looped back in the windings, as shown in Figure 13. This coil is clamped on to the conductor which we are sensing, as shown in Figure 14.

There are two kinds of coils available in the market: flexible RCs and rigid RCs. Depending on where we require to place them, any of these can be chosen. We have used flexible RCs.

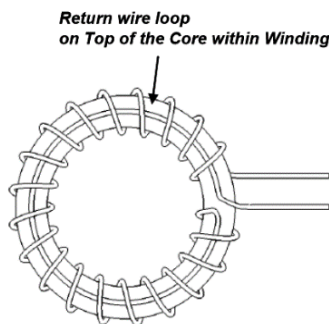


Figure 13. Rogowski Coil design



Figure 14. Coil around conductor

E. Working Principle of the Rogowski Coil

When a coil is wrapped around the conductor as shown in Figure 14, and the conductor is passing a current in the range of what the coil can measure, it will give an output voltage that is proportional to the change in current in the conductor. Whenever there is a change in the current flowing through the conductor, the output of the coil changes according to this equation:

$$u(t) = e(t) = - M \cdot \frac{di}{dt} \quad (1)$$

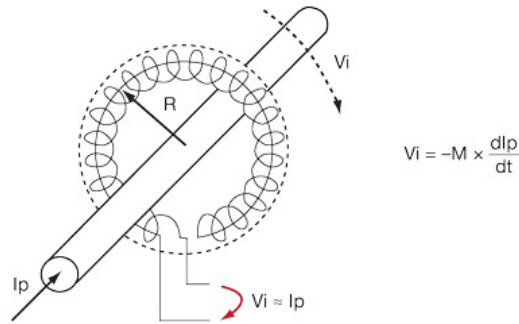


Figure 15. Principle of operation

Therefore, we know that the output voltage is dependent on the mutual inductance of the coil and rate of change of current in the conductor. It is clear that this has a differential output, thus a simple integrator circuit is needed at the output of the coil to get the output we are looking for (figures 15 and 16). Since the coil has an air core, the mutual inductance is low, thus sometimes we might require to amplify the output to get a higher voltage signal out of the coil.

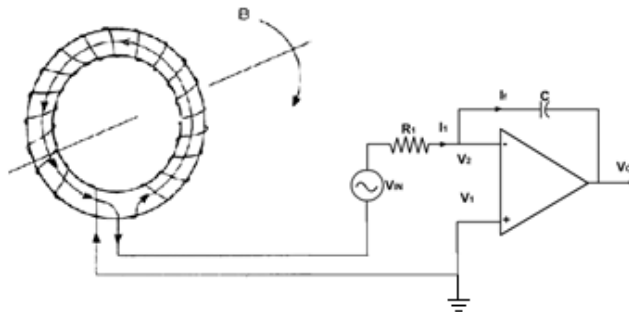


Figure 16. Rogowski Coil with integrator

F. Implementation

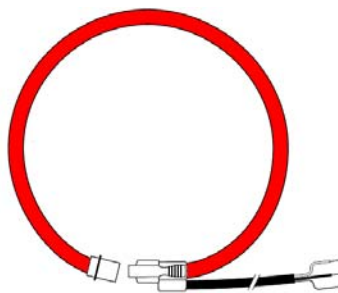


Figure 17. Rogowski Coil with brown, white and shield

A 4.17” window size coil, the Accuenergy RCT16 is used in this application. Testing is done using a programmable load, Chroma 63802. The Rogowski coil is clamped around the I-output cable. The output of the coil consists of three wires which is given to an integrator circuit, the brown wire is the positive wire and

is connected to the resistor R1, and the negative (white wire) and the shield are connected to the ground (Figure 17). A sine wave is obtained at V_0 , which is then converted to DC voltage.

For conversion of the AC signal to DC, a positive clamping circuit is used (Figure 18). The clamping circuit clamps the negative half of the sine wave and passes the positive half of it, along with raising the signal by a level of 0.7V using a DC supply. The output of this circuit is given to a low-pass filter which then smoothens this out to a perfect DC signal. The circuit put together for this is shown in Figure 19.

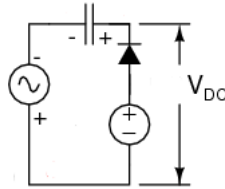


Figure 18. Positive clamper

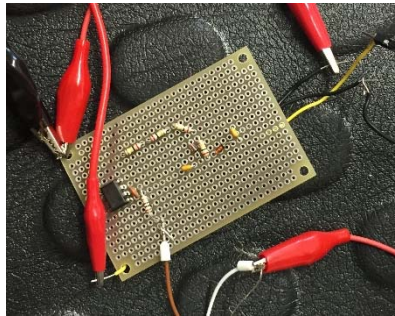


Figure 19. Integrator, clamper and envelope detector circuits

This signal is given to a data acquisition board MDA300CA (Figure 20).



Figure 20. MDA300CA Board

The MDA300CA board is interfaced with a MicaZ mote. The DC signal from the circuit shown above is given as input to this board. The output voltage is read and the relation between the output voltage and the current in the conductor is calculated. Therefore, the current in the conductor can be calculated without much error. The same as in the case of tilt sensor, these MicaZ motes connected to the coils are considered to be end-device motes. They collect data and send it to the coordinator mote.

G. Advantages of Using Rogowski Coil as a Line Sensor

In almost all line current sensing applications, current transformers are used. These devices have various advantages over other types of sensors, especially in the power grid application. However, they have several

disadvantages too. For example, since the current transformers have an iron core, there is room for saturation when there are high currents running through the line, or if there are continuous changes in the current in the conductor. Also it is heavy and bulky. Another disadvantage of split core CTs is that it is expensive. It is also more susceptible to external noise. An open-circuited CT is very dangerous, as it can produce lethal voltages. The high voltage across the secondary winding could also cause insulation failure in that winding, either leading to inaccuracy, a burn-out or a fire.

After careful planning and research, Rogowski coils were chosen since they have many advantages over conventional current transformers and other such current sensors. These are as listed: Rogowski coils are safer compared to CTs, while installation or repair. They have no core losses, and are light weight and very easy to install without the risk of starting a fire or burning it out as in CTs. They are highly linear over a wide range of currents, thus no saturation like in current transformers (Figure 21). These coils are compact and light weight. The output of the Rogowski coil is low enough not to cause any hazardous voltages which is the case in CTs. Rogowski coils can be open circuited without any hazardous effects. The efficiency and accuracy of the sensor is high when compared with current transformers. In addition, there are no losses in the secondary cabling, also no core losses since it has an air core. Since it has low inductance, it responds to very fast changing currents. It is also not susceptible to external noise. The Rogowski coil is easy to install since it is a clamp-on.

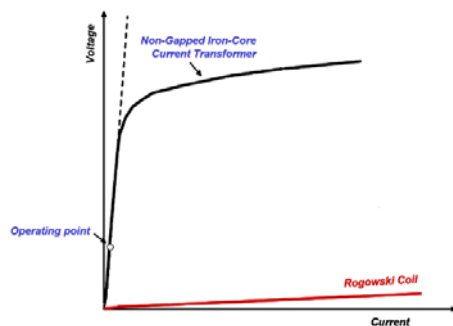


Figure 21. Linearity of the Rogowski Coil vs CTs

However, it has its own disadvantages. The output of the coil is a derivative of the primary current in the conductor (di_p/dt). Thus to obtain the power frequency signal, some signal processing is required. To overcome this, we use an integrator circuit. We can conclude that even though the coil has some disadvantages, they can be overcome easily at a low cost.

6. OPTIMIZATION

The optimization portion of this project seeks to take the data acquired by sensors spread throughout a distribution system and determine the optimal configuration that maximizes the connectivity of prioritized load. Below is a detailed description of the formulation of a Mixed Integer Linear Program (MILP) adapted from [18]. Also integration of MILP method with the openDSS [19] is introduced. Then the MILP is applied on a reduced version of a utility feeder (*Appendix A*). Finally, a comparison between the MILP and the openDSS results is presented.

A. Methodology: Optimization Problem Formation for Radial Distribution Systems to Supply Critical Loads (CLs) from Distributed Energy Resources (DERs) and Increase Resiliency

Figure 22 illustrates the MILP variables used in this section. Let a distribution system be represented by its nodes and sections denoted by N and S such that

$$N: = \{1, \dots, n\}$$

$$S := \{(i, j)\} \subseteq N \times N$$

where n is the number of nodes in the system. Also suppose that located in this system there are m DERs located at nodes d_1, d_2, \dots, d_m which have the ability to form m isolated micro-grids, each containing only one DER. Let the set of nodes containing DERs be

$$D := \{d_1, d_2, \dots, d_m\} \subseteq N$$

and the nodes and sections belonging to the k^{th} micro-grid be N_{d_k} and S_{d_k} respectively. For simplification, let each micro-grid be defined by the node where the DER is located. In other words, The set containing all micro-grids G , is defined:

$$Z \triangleq D$$

Note that a substation transformer can be considered among these distributed energy resources and that under normal operation $D = \{B\}$, $N_B = N$, and $S_B = S$ where B is the node connected to the substation transformer and all other DERs have been deactivated.

Parameters (given):

1. Each node i has an associated demand of real and reactive power denoted p_i and q_i . If the system has no load attached at node i , then $p_i = q_i = 0$.
2. Each edge (i, j) has an associated resistance and reactance denoted r_{ij} and x_{ij} .
3. Each DER has a maximum real and reactive power capacity that it can supply to its surrounding nodes. Let the real and reactive power capacity of the DER located at node d be denoted P_d^{max} and Q_d^{max} .
4. The systems nominal line-to-ground Voltage will be represented by the constant V_R and the tolerance allowed on this voltage will be represented by the constant ϵ . Typical values for a $12.47kV$ distribution system would be $V_R = 7.2kV$ and $\epsilon = 5\%$.
5. Each edge (i, j) also has a maximum amount of current that it can allow to flow through denoted I_{ij}^{max} .
6. Each node i has an associated weight denoted w_i which will be used to prioritize the order in which loads are considered. It should be noted that the optimization will take the product of this weight and the demand p_i , so the higher priority loads should have a weight large enough to overcome a higher demand by a lower priority load. The actual formation of these weights is not discussed in this problem, however, and the weights are assumed to be given.

Variables:

1. Each node is assumed to have the ability to disconnect or reconnect from the load located at that node. Let a_i be a binary variable that stores the state of this switch at node i where

$$a_i := \begin{cases} 1 & p_i \text{ and } q_i \text{ connected to node } i \\ 0 & p_i \text{ and } q_i \text{ disconnected from node } i \end{cases}$$

2. Likewise each section is assumed to have the ability to disconnect or reconnect its two adjacent nodes. Let b_{ij} be a binary variable that stores the state of this switch where

$$b_{ij} := \begin{cases} 1 & \text{nodes } i \text{ and } j \text{ are connected} \\ 0 & \text{nodes } i \text{ and } j \text{ are disconnected} \end{cases}$$

* Note that if a particular node or edge does not have this ability, the problem can be constrained in such a way that accurately represents the system using the Distribution System Condition Constraints (DSCC) below.

3. Ultimately, the goal is to determine which loads are being supplied by which micro-grids. Therefore let the binary variable c_{id} be defined in the following way to determine if a given load is being supplied by a given micro-grid.

$$c_{id} := \begin{cases} 1 & \text{the load at node } i \text{ is being supplied by microgrid } d \\ 0 & \text{the load at node } i \text{ is not being supplied by microgrid } d \end{cases}$$

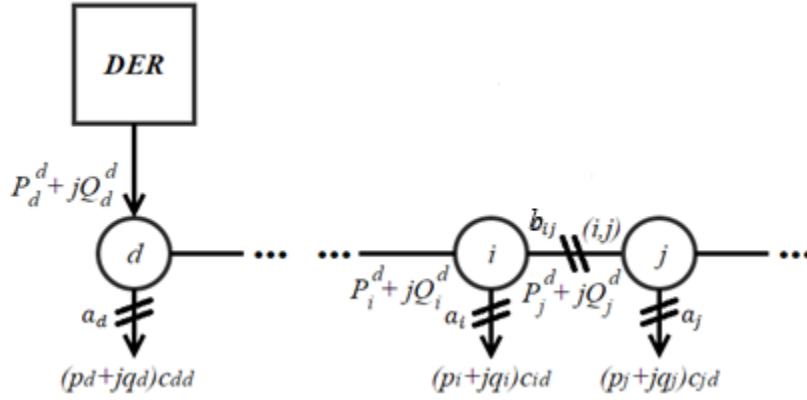


Figure 22. MILP variables

Formulation:

The maximization problem seeks to maximize the amount of prioritized load that can be picked up by each DER. By summing through all of the possible sources of power, we can determine the load supplied at node i to be $\sum_{d \in D} c_{id} p_i$. Note that $\sum_{d \in D} c_{id} p_i = 0$ for any node not belonging to a micro-grid or disconnected from its load. Summing through all of the nodes in the system and using the weights to prioritize load, the maximization problem becomes:

$$\max_{a_i, b_{ij}, c_{id}, \gamma_{id}} \sum_{i \in N} w_i \sum_{d \in D} c_{id} p_i$$

Constraints:

1. Distribution System Condition Constraints (DSCC)

First we must consider the current condition of the Distribution System. Certain nodes may be either permanently or temporarily connected or disconnected from its respective load due to either the configuration of the system, faults, or equipment failure. Likewise, certain sections may be either permanently or temporarily connected or disconnected. Let N_O , N_C , S_O , and S_C contain all the nodes whose loads are locked in the connected or disconnected state and all of the sections that are locked in the connected or disconnected state respectively. Then the DSCC can be written as

$$\begin{aligned} a_i &= \mathbf{0}, \forall i \in N_O \\ a_i &= \mathbf{1}, \forall i \in N_C \\ b_{ij} &= \mathbf{0}, \forall (i, j) \in S_O \\ b_{ij} &= \mathbf{1}, \forall (i, j) \in S_C \end{aligned}$$

2. Load Pickup Constraints (LPC)

Let the binary variable γ_{id} be defined in the following way to determine if a given node is connected to a given micro-grid.

$$\gamma_{id} = \begin{cases} 1 & \text{node } i \text{ is connected to zone } d \\ 0 & \text{node } i \text{ is not connected to zone } d \end{cases}$$

Due to the fact that a load must be connected to the node that it is located at and that node must be connected to a given micro-grid, in order for that load to be supplied by the given micro-grid, the quadratic relationship between a_i , c_{id} and γ_{id} is described by the following:

$$c_{id} = a_i \gamma_{id}, \forall i \in N, d \in D$$

This can be simplified into the following three linear inequalities:

$$\begin{aligned} c_{id} &\leq \gamma_{id}, \forall i \in N, d \in D \\ c_{id} &\leq a_i, \forall i \in N, d \in D \\ c_{id} &\geq \gamma_{id} + a_i - 1, \forall i \in N, d \in D \end{aligned}$$

3. Zone Standalone Constraint (ZSC):

Because each micro-grid must be a standalone system, we must have the following:

$$\begin{aligned} \forall d \in D, \quad N_d \subset N \text{ and } S_d \subset S \\ \forall d_1, d_2 \in D, \quad N_{d_1} \cap N_{d_2} = \emptyset \text{ and } S_{d_1} \cap S_{d_2} = \emptyset \end{aligned}$$

This can be satisfied by ensuring that all nodes can only belong to at most one micro-grid.

$$\sum_{d \in D} \gamma_{id} \leq 1, \forall i \in N$$

We also must consider that the nodes where DERs are located must belong to their own respective micro-grids.

$$\gamma_{id} = 1, \forall i \in N, d \in D \text{ s.t. } i = d$$

We also must consider the parent-child relationships of each node with respect to the micro-grid that it is located in. Since we are discussing radial configurations, every node will have exactly one parent node with respect to a given micro-grid with the exception of the node located at the DER for that micro-grid. If a node is located in a given micro-grid, it must also be true that that node's parent node with respect to the given micro-grid is also located in that same micro-grid. Let $\theta_d(i)$ denote the parent node of node i with respect to micro-grid d . Then

$$\gamma_{id} \leq \gamma_{jd}, \forall d \in D, i \in N \setminus \{d\}, j = \theta_d(i)$$

Likewise, every parent-child pair located in the same micro-grid must have a connected edge between them. This along with the previous constraint means that every edge with a child node located in a given micro-grid must be closed. Let $\zeta_d(i, j)$ denote the child node of edge (i, j) with respect to micro-grid d . Then

$$b_{ij} = \sum_{d \in D} \gamma_{hd}, \forall (i, j) \in S, h = \zeta_d(i, j)$$

4. Power/Voltage/Current Constraints (PVCC)

*Uses Linearized DistFlow model (same as paper)

a. Real and Reactive Power Balance

Let P_i^d and Q_i^d denote the real and reactive power flow into node i supplied from micro-grid d .

$$\begin{aligned} \sum_{j \in J_i^d} P_j^d &= P_i^d - c_{id} p_i, \forall d \in D, i \in N \\ \sum_{j \in J_i^d} Q_j^d &= Q_i^d - c_{id} q_i, \forall d \in D, i \in N \end{aligned}$$

Where J_i^d denotes the set of children nodes of node i with respect to micro-grid d . Note that for any node i not located in micro-grid d (i.e., $\gamma_{id} = 0$), $P_i^d = Q_i^d = 0$. Also note that the power flow cannot exceed the capacity of the DER. This is represented by the following inequality constraints:

$$\begin{aligned} 0 \leq P_i^d &\leq \gamma_{id} P_d^{\max}, \forall d \in D, i \in N \\ 0 \leq Q_i^d &\leq \gamma_{id} Q_d^{\max}, \forall d \in D, i \in N \end{aligned}$$

b. Voltage Constraints

Let V_i^d be the voltage at node i supplied by micro-grid d and V_d^d , the voltage at the DER in micro-grid d , be set to the reference voltage

$$\begin{aligned} V_d^d &= V_R, \forall d \in D \\ V_i^d &= V_j^d - \frac{r_{ij} P_i^d + x_{ij} Q_i^d}{V_d^d} - \delta_i^d, j = \theta_d(i), i \in N \setminus \{d\}, d \in D \end{aligned}$$

where δ_i^d is a slack variable to handle cases when node i is not part of micro-grid d , but parent node j is. The constraints for δ_i^d can be written as

$$0 \leq \delta_i^d \leq (1 - \gamma_{id}) V_d^d, \forall i \in N, d \in D$$

Note that for any node i not located in micro-grid d (i.e. $\gamma_{id} = 0$), $V_i^d = 0$. Also note that the voltage at any child node will be less than the voltage at its parent node. This is represented by the following inequality constraints:

$$\mathbf{0} \leq V_i^d \leq \gamma_{id} V_0^d, \forall d \in \mathbf{D}, i \in \mathbf{N}$$

The actual voltage at any node then can be expressed as $\sum_{d \in \mathbf{D}} V_i^d$ and so, with reference voltage V_R and tolerance ϵ , the voltage constraint becomes

$$V_R(1 - \epsilon) \leq \sum_{d \in \mathbf{D}} V_i^d \leq V_R(1 + \epsilon), \forall i \in \mathbf{N}$$

c. Current Constraints

To simplify the problem, constraining the current will be done through the power flow variables that we have already developed.

$$\mathbf{0} \leq P_j^d \leq \gamma_{jd} P_{ij}^{max}, j = \zeta_d(i, j), \forall (i, j) \in \mathbf{S}, d \in \mathbf{D}$$

where P_{ij}^{max} is the maximum power allowed to flow through edge (i, j) derived from the formula $P_{ij}^{max} = I_{ij}^{max} V_R(1 - \epsilon)$

B. Integration of MILP with OpenDSS

In order to verify the validity of the MILP Results, the linearized power flow model used will need to be compared against a more rigorous power flow simulator. For this project OpenDSS was explored as an option for power flow simulation. OpenDSS is an open sourced Distribution System Simulator (DSS) developed by EPRI that runs most analyses that utilities use to study distribution systems while also offering functionality specifically for technological advancements occurring in the grid such as smart grid technologies and PV penetration. The GridPV toolbox, also developed by EPRI, is a set of tools in MATLAB that allow a user to control simulations and collect data from OpenDSS in the MATLAB interface. This toolbox was used so that analysis of the power flow results could be done in MATLAB.

Figure 23 shows an illustration of the interaction between MATLAB and OpenDSS as well as a proposed flow chart for decisions to be made regarding the outputs of both the MILP and OpenDSS. In this figure, the MILP results the voltage at each node and real and reactive power through each section. These power flow results are compared to the power flow results of the OpenDSS. The error can be applied to modify the MILP constraints in order to get close results with the OpenDSS.

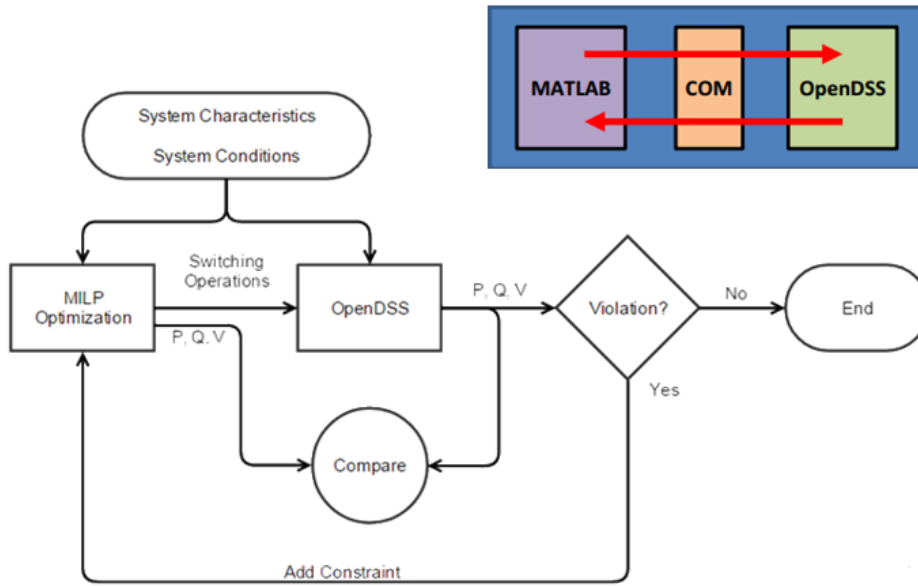


Figure 23. OpenDSS and MATLAB Interface

C. Results

Figure 23 below shows the results obtained by running the MILP on a test feeder with the following specifications: (1) Source, (2) Circuit Ties, (6) DERs, (124) Nodes, (123) Sections, (1) Recloser, (15) Switches, (29) Fuses, and (85) Spot Loads. Tables showing load values and other information are shown in *Appendix B*. The micro-grids outlined by the dotted lines are dynamically formed around each DER by the MILP. Notice that there are 6 isolated micro-grids formed around each of the 6 DER's. This is a direct result of the Zone Standalone Constraints. Also notice that some loads were not served in micro-grids 4 and 5. This was due to the Power/Voltage/Current Constraints which limit the capacity of the DERs.

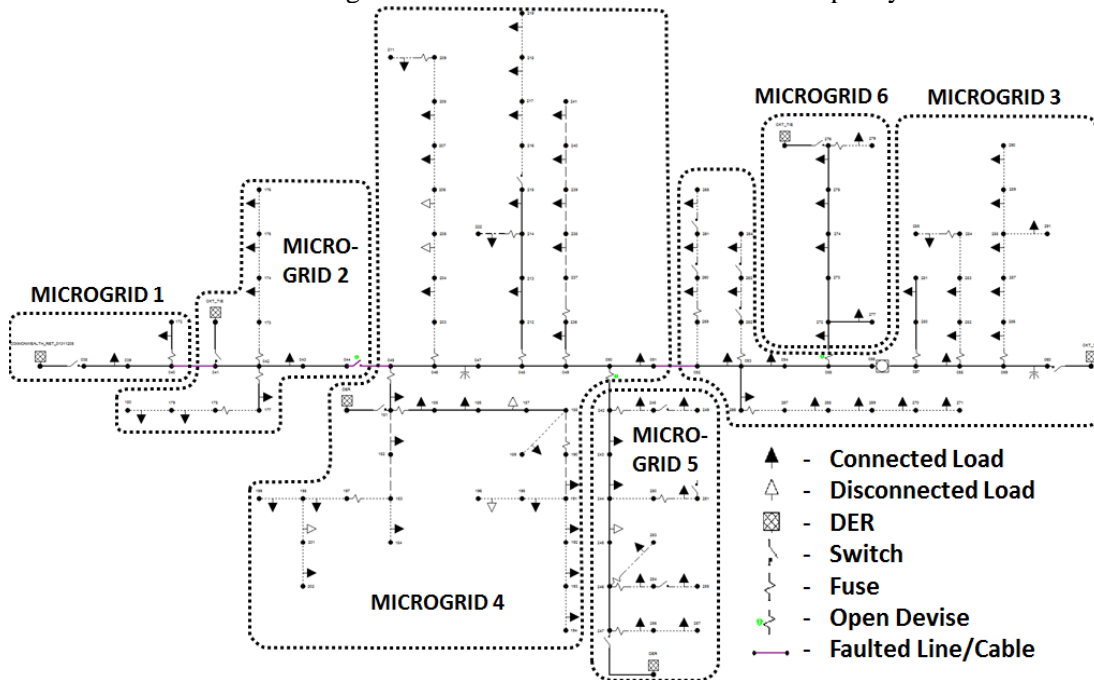


Figure 24. MILP Optimization Results on Test Feeder

In order to test the results of the MILP, power flow was simulated on a test feeder with the following specifications: (1) Source: Commonwealth Sub, (1) Circuit Tie, (2) Reclosers, (2) Shunt Capacitors, (18) Switches, (86) Fuses, (289) Loads, (686) Nodes, (694) Sections. It should also be noted that the only generation point considered was the substation and that the circuit was under normal operation with no faulted sections. Figure 25 below shows the results from this test. The slight difference in calculation can be attributed to the linearization of the power flow in the MILP, however, the similarity in shape of the curves validates the operation of the MILP in the normal operation case.

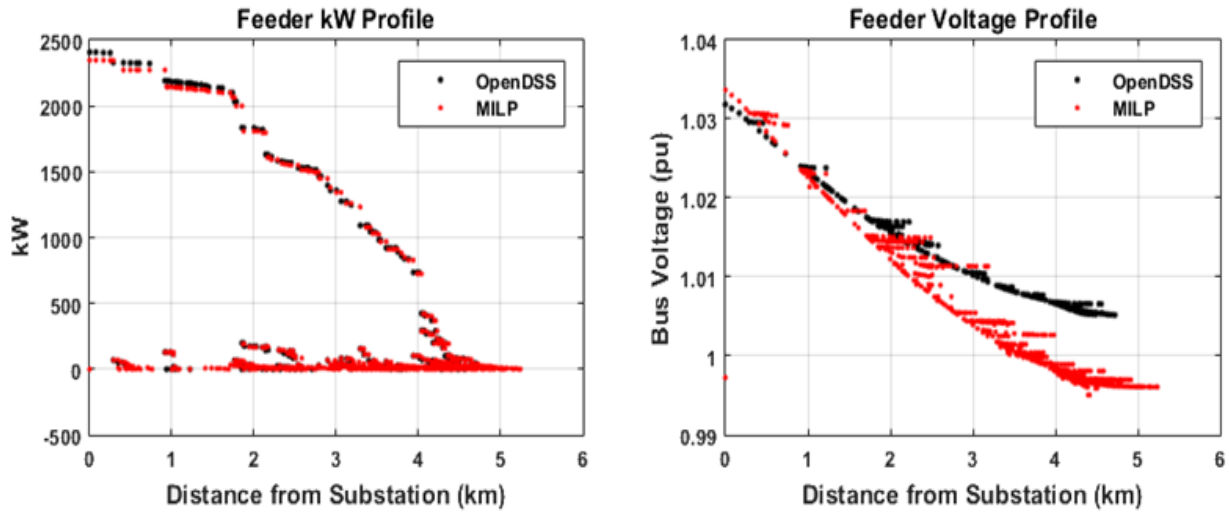


Figure 25. Comparison of MILP and OpenDSS Power Flow

1. Conclusion and Future Work

In conclusion, the MILP has been tested for various fault conditions and the outputs for a base case have been compared to a static power flow in OpenDSS. The results of this testing have shown that it is a strong tool for configuration of a circuit in a fault situation. Further testing will be required to test the MILP in different dynamic scenarios.

Moving forward, we hope to be able to expand on the interface between OpenDSS and MATLAB so that switching controls can be sent from MATLAB to OpenDSS. It is also a goal to explore the effects of islanding in the system and the effects of dynamic load modeling which will both be possible through OpenDSS. Finally, we will need to study what types of DER will work with this type of model and address the variability issue of DER like wind and PV.

7. CONCLUSION AND FUTURE WORK

We have built and tested a system that accurately and efficiently reports the health of the power poles and lines. We have made use of low-cost components to implement this. It consists of three tiers: one consisting of the sensors, second consisting of ZigBee network and third comprising of the GSM communication and visualization system.

In future research, we will incorporate methods to efficiently power the components we make use of, and try to reduce the power consumption as much as possible. We intend to develop a system for actual demonstration in a working feeder. We will also make our wireless communication network compatible with the DNP3 interface for smart grid compatibility.

ACKNOWLEDGEMENT

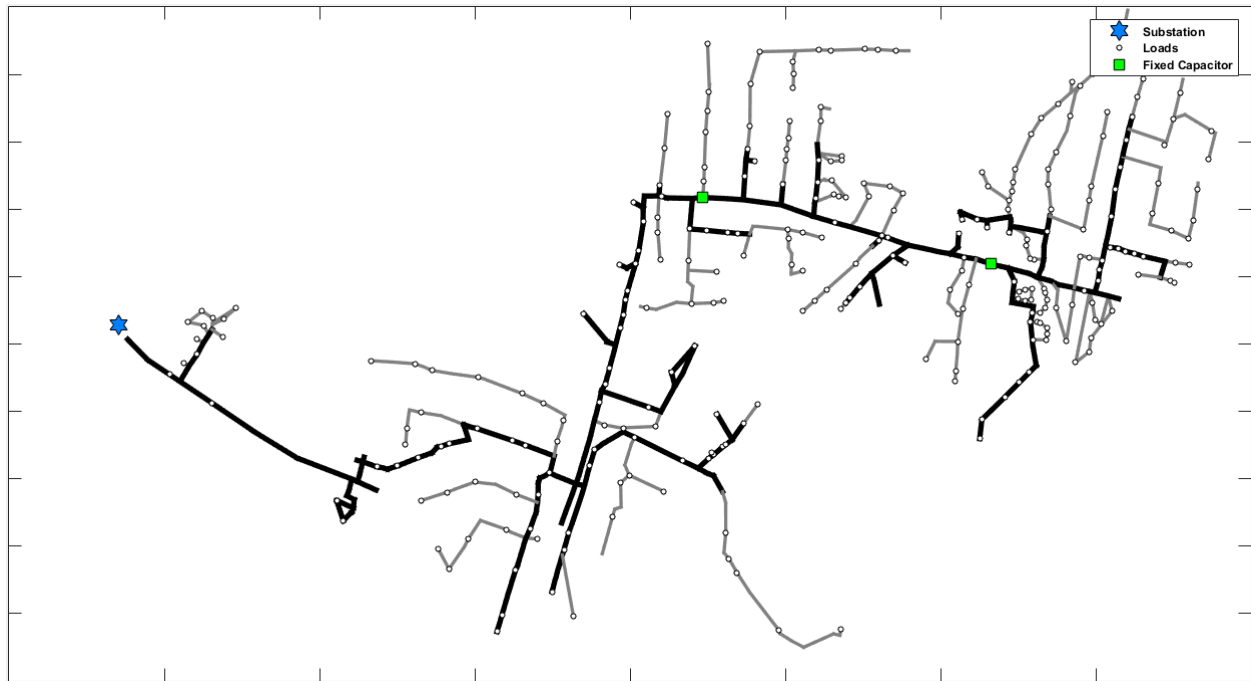
This work is supported by Center for Advanced Power Engineering Research (CAPER).

REFERENCES

- [1] Wireless Sensor Networks, “MTS/MDA Sensor Board User’s Manual”, 2004, Crossbow Technology, Inc.
- [2] Wireless Sensor Networks, “MPR/MIB User’s Manual”, 2004, Crossbow Technology, Inc.
- [3] Power System Relaying Committee of the IEEE PES, “Practical Aspects of Rogowski Coil Applications to Relaying”, Sept. 2010.
- [4] <https://www.accuenergy.com/files/acuct/RCT-Rogowski-coil-flexible-current-transformer-brochure.pdf>
- [5] D. A. Ward and J. La T. Exon, “Using Rogowski Coils for Transient Current Measurements”, Engineering Science and Education Journal, June 1993.
- [6] Zhou Li, Qiaogen Zhang, Lu Zhang, Fenglian Liu, Xiaoya Tan, “Design of Rogowski Coil with external integrator for measurement of lightning current up to 400kA”, July 2011.
- [7] L. Di Rienzo, A. Ferrero and R. Ottoboni, “Balanced Front-End Electronics for Rogowski Coils”.
- [8] Yong Ouyang, Jinliang He, Jun Hu and Shan X. Wang, “A Current Sensor Based on the Giant Magnetoresistance Effect: Design and Potential Smart Grid Applications”, Sensors 2012, ISSN 1424-8220.
- [9] <http://www.tollgrade.com/smartgrid/smart-grid-products/smart-grid-mv-sensor/>
- [10] ENERGY 2013: The Third International Conference on Smart Grids, Green Communications and IT Energy-aware Technologies. Francisc Zavoda, Canada, Chris Yakymyshyn, USA, “Sensors for Smart Grids”, Smart Grids Technologies.
- [11] “GridAdvisor Series II smart sensor”, Cooper Power Systems by Eaton, June 2014.
- [12] António Grilo, Helena Sarmento, Mário Nunes, José Gonçalves, Paulo Pereira, Augusto Casaca, Carlos Fortunato, “A Wireless Sensors Suite for Smart Grid Applications”, 2011.
- [13] Paul Doig, “Smart Sensors Enable a Smarter Grid Improving High Voltage Grid Reliability through the use of readily deployable, distributed, wireless intelligent sensors”, Schneider Electric, 2006.
- [14] Wang Na, Wan Quan, “Application of the Fiber Optical Current Transformer in the 110kV Smart Substation”, 2012.
- [15] William Koon, “Current Sensing for Energy Metering”, Analog Devices, Inc.
- [16] <http://cpham.perso.univ-pau.fr/WSN/iMote-XBee.html>
- [17] TylerW. Davis, Xu Liang, Miguel Navarro, Diviyansh Bhatnagar, and Yao Liang, “An Experimental Study of WSN Power Efficiency: MICAz Networks with XMesh”, 20 October 2011.
- [18] Chen, C., Wang, J., Qui, F., & Zhao, D. (2015). Resilient distribution system by microgrids formation after natural disasters, *IEEE Trans. Smart Grid.* , 1-1. Doi: 10.1109/TSG.2015.2429653
- [19] Open Distribution System Simulator (OpenDSS), EPRI, June 2013.

Appendix A: Test Feeder for Optimization

Below is the test feeder considered for this project. The feeder has the following specifications: (686) Nodes, (694) Section, (289) Loads [(359) by phase], (86) Fuses, (18) Switches, (2) Reclosers, (1) Source, (2) Capacitors



Commonwealth Ckt 01311205

Appendix B: MILP Circuit Data and Results for Optimization Routine

Code	Node Id	Node Data		Emergency Priority
		Total kW	Total kvar	
Node	038	0	0	0
Node	039	24.68	5.08	1
Node	040	0	0	0
Node	041	0	0	0
Node	042	0	0	0
Node	043	17.92	3.49	1
Node	044	0	0	0
Node	045	0	0	0
Node	046	0	0	0
Node	047	0	0	0
Node	048	0	0	0
Node	049	0	0	0
Node	050	0	0	0
Node	051	3.58	0.7	3
Node	052	0	0	0
Node	053	24.68	5.08	1
Node	054	8.96	1.75	3
Node	055	0	0	0

Node	056	0	0	0
Node	057	0	0	0
Node	058	7.23	1.67	1
Node	059	0	0	0
Node	060	0	0	0
Node	172	24.68	5.08	1
Node	173	0	0	0
Node	174	7.23	1.67	1
Node	175	14.45	3.34	1
Node	176	14.45	3.34	1
Node	177	49.36	10.17	2
Node	178	0	0	0
Node	179	16.99	3.34	3
Node	180	16.99	3.34	3
Node	181	8.96	1.75	2
Node	182	7.23	1.67	2
Node	183	0	0	0
Node	184	14.45	3.34	2
Node	185	8.96	1.75	3
Node	186	24.68	5.08	3
Node	187	7.23	1.67	1
Node	188	0	0	0
Node	189	17.92	3.49	2
Node	190	0	0	0
Node	191	8.96	1.75	3
Node	192	5.37	1.05	1
Node	193	5.37	1.05	3
Node	194	17.92	3.49	2
Node	195	16.99	3.34	2
Node	196	25.48	5	1
Node	197	0	0	0
Node	198	8.49	1.67	3
Node	199	8.49	1.67	3
Node	201	8.49	1.67	1
Node	202	8.49	1.67	2
Node	203	0	0	0
Node	204	14.45	3.34	2
Node	205	14.45	3.34	1
Node	206	7.23	1.67	1
Node	207	7.23	1.67	1
Node	208	14.45	3.34	3
Node	209	0	0	0
Node	211	48.28	11.16	1
Node	212	0	0	0
Node	213	8.49	1.67	2
Node	214	0	0	0
Node	215	9.87	2.03	2
Node	216	0	0	0
Node	217	16.99	3.34	2
Node	218	16.99	3.34	3
Node	219	16.99	3.34	3

Node	222	49.36	10.17	2
Node	236	9.87	2.03	3
Node	237	0	0	0
Node	238	17.92	3.49	1
Node	239	17.92	3.49	3
Node	240	16.99	3.34	2
Node	241	16.99	3.34	1
Node	242	0	0	0
Node	243	7.23	1.67	3
Node	244	7.23	1.67	1
Node	245	14.45	3.34	1
Node	246	0	0	0
Node	247	0	0	0
Node	248	59.84	11.67	2
Node	249	59.84	11.67	2
Node	250	0	0	0
Node	251	59.84	11.67	2
Node	252	59.84	11.67	3
Node	253	56.73	11.14	2
Node	254	56.73	11.14	3
Node	255	56.73	11.14	1
Node	256	7.23	1.67	3
Node	257	14.45	3.34	3
Node	259	0	0	0
Node	260	48.28	11.16	3
Node	261	28.91	6.68	3
Node	262	0	0	0
Node	263	48.28	11.16	1
Node	264	48.28	11.16	1
Node	265	48.28	11.16	3
Node	266	24.68	5.08	2
Node	267	0	0	0
Node	268	14.45	3.34	3
Node	269	7.23	1.67	2
Node	270	7.23	1.67	2
Node	271	7.23	1.67	3
Node	272	17.92	3.49	3
Node	273	0	0	0
Node	274	24.68	5.08	3
Node	275	24.68	5.08	1
Node	276	24.68	5.08	1
Node	277	74.03	15.25	1
Node	279	7.23	1.67	2
Node	280	0	0	0
Node	281	74.03	15.25	1
Node	282	17.92	3.49	1
Node	283	17.92	3.49	3
Node	284	0	0	0
Node	285	59.84	11.67	1
Node	286	5.37	1.05	1
Node	287	17.92	3.49	1

Node	288	17.92	3.49	3
Node	289	8.96	1.75	1
Node	290	8.96	1.75	3
Node	291	8.96	1.75	3

Parent Node Function:	DER 038 (MAIN FEED)	DER 041 (CKT TIE1)	DER 060 (CKT TIE2)	DER 181 (DER1)	DER 247 (DER2)	DER 276 (DER3)
	NONE	039	039	039	039	039
	038	040	040	040	040	040
	039	041	041	041	041	041
	040	NONE	042	042	042	042
	041	041	043	043	043	043
	042	042	044	044	044	044
	043	043	045	045	045	045
	044	044	046	181	046	046
	045	045	047	045	047	047
	046	046	048	046	048	048
	047	047	049	047	049	049
	048	048	050	048	050	050
	049	049	051	049	242	051
	050	050	052	050	050	052
	051	051	053	051	051	053
	052	052	054	052	052	054
	053	053	055	053	053	055
	054	054	056	054	054	272
	055	055	057	055	055	055
	056	056	058	056	056	056
	057	057	059	057	057	057
	058	058	060	058	058	058
	059	059	NONE	059	059	059
	040	040	040	040	040	040
	042	042	042	042	042	042
	173	173	173	173	173	173
	174	174	174	174	174	174
	175	175	175	175	175	175
	042	042	042	042	042	042
	177	177	177	177	177	177
	178	178	178	178	178	178
	179	179	179	179	179	179
	045	045	045	NONE	045	045
	181	181	181	181	181	181
	182	182	182	182	182	182
	183	183	183	183	183	183
	181	181	181	181	181	181
	185	185	185	185	185	185
	186	186	186	186	186	186
	187	187	187	187	187	187
	188	188	188	188	188	188
	188	188	188	188	188	188
	190	190	190	190	190	190

191	191	191	191	191	191
192	192	192	192	192	192
193	193	193	193	193	193
191	191	191	191	191	191
195	195	195	195	195	195
183	183	183	183	183	183
197	197	197	197	197	197
198	198	198	198	198	198
198	198	198	198	198	198
201	201	201	201	201	201
046	046	046	046	046	046
203	203	203	203	203	203
204	204	204	204	204	204
205	205	205	205	205	205
206	206	206	206	206	206
207	207	207	207	207	207
208	208	208	208	208	208
209	209	209	209	209	209
048	048	048	048	048	048
212	212	212	212	212	212
213	213	213	213	213	213
214	214	214	214	214	214
215	215	215	215	215	215
216	216	216	216	216	216
217	217	217	217	217	217
218	218	218	218	218	218
214	214	214	214	214	214
049	049	049	049	049	049
236	236	236	236	236	236
237	237	237	237	237	237
238	238	238	238	238	238
239	239	239	239	239	239
240	240	240	240	240	240
050	050	050	050	243	050
242	242	242	242	244	242
243	243	243	243	245	243
244	244	244	244	246	244
245	245	245	245	247	245
246	246	246	246	NONE	246
242	242	242	242	242	242
248	248	248	248	248	248
244	244	244	244	244	244
250	250	250	250	250	250
251	251	251	251	251	251
246	246	246	246	246	246
246	246	246	246	246	246
254	254	254	254	254	254
247	247	247	247	247	247
256	256	256	256	256	256
052	052	052	052	052	052
259	259	259	259	259	259

260	260	260	260	260	260	260
053	053	053	053	053	053	053
262	262	262	262	262	262	262
263	263	263	263	263	263	263
261	261	261	261	261	261	261
053	053	053	053	053	053	053
266	266	266	266	266	266	266
267	267	267	267	267	267	267
268	268	268	268	268	268	268
269	269	269	269	269	269	269
270	270	270	270	270	270	270
055	055	055	055	055	055	273
272	272	272	272	272	272	274
273	273	273	273	273	273	275
274	274	274	274	274	274	276
275	275	275	275	275	275	NONE
272	272	272	272	272	272	272
276	276	276	276	276	276	276
057	057	057	057	057	057	057
280	280	280	280	280	280	280
058	058	058	058	058	058	058
282	282	282	282	282	282	282
283	283	283	283	283	283	283
284	284	284	284	284	284	284
059	059	059	059	059	059	059
286	286	286	286	286	286	286
287	287	287	287	287	287	287
288	288	288	288	288	288	288
289	289	289	289	289	289	289
288	288	288	288	288	288	288

DER Nodes:	Node Id	DER Capacity kVA
	038	4000000
	041	4000000
	060	4000000
	181	500
	247	500
	276	500

Code	Section Data						
	From Node	To Node	Line R1 Ohms	Line X1 Ohms	Capacity Max (A)	Has Switching Device	Switching State
Overhead Line By Phase	038	039	0.001	0.003	560	FALSE	
Overhead Line By Phase	039	040	0.007	0.016	560	FALSE	
Overhead Line By Phase	040	041	0.006	0.014	560	FALSE	

Overhead Line By Phase	041	042	0.008	0.019	560	FALSE	
Overhead Line By Phase	042	043	0.001	0.003	560	FALSE	
Overhead Line By Phase	043	044	0.003	0.007	560	FALSE	
Overhead Line By Phase	044	045	0.014	0.033	560	TRUE	Close
Overhead Line By Phase	045	046	0.006	0.014	560	FALSE	
Overhead Line By Phase	046	047	0.013	0.03	560	FALSE	
Overhead Line By Phase	047	048	0.01	0.023	560	FALSE	
Overhead Line By Phase	048	049	0.021	0.05	560	FALSE	
Overhead Line By Phase	049	050	0.019	0.045	560	FALSE	
Overhead Line By Phase	050	051	0.012	0.028	560	FALSE	
Overhead Line By Phase	051	052	0.009	0.02	560	FALSE	
Overhead Line By Phase	052	053	0.019	0.043	560	FALSE	
Overhead Line By Phase	053	054	0.003	0.008	560	FALSE	
Overhead Line By Phase	054	055	0.012	0.028	560	FALSE	
Overhead Line By Phase	055	056	0.018	0.041	560	FALSE	
Overhead Line By Phase	056	057	0.006	0.015	560	TRUE	Close
Overhead Line By Phase	057	058	0.008	0.019	560	FALSE	
Overhead Line By Phase	058	059	0.007	0.016	560	FALSE	
Overhead Line By Phase	059	060	0.009	0.02	560	FALSE	
Overhead Line By Phase	040	172	0.029	0.016	40	TRUE	Close
Overhead Line By Phase	042	173	0.002	0.001	20	TRUE	Close
Overhead Line By Phase	173	174	0.093	0.056	130	FALSE	
Overhead Line By Phase	174	175	0.067	0.041	130	FALSE	
Overhead Line By Phase	175	176	0.055	0.06	260	FALSE	
Overhead Line By Phase	042	177	0.025	0.014	80	TRUE	Close
Overhead Line By Phase	177	178	0.009	0.008	50	TRUE	Close

Overhead Line By Phase	178	179	0.101	0.086	198	FALSE	
Overhead Line By Phase	179	180	0.101	0.079	198	FALSE	
Overhead Line By Phase	045	181	0.123	0.046	80	TRUE	Close
Overhead Line By Phase	181	182	0.128	0.052	130	FALSE	
Overhead Line By Phase	182	183	0.038	0.015	130	FALSE	
Overhead Line By Phase	183	184	0.137	0.075	130	FALSE	
Overhead Line By Phase	181	185	0.074	0.028	65	TRUE	Close
Overhead Line By Phase	185	186	0.091	0.034	130	FALSE	
Overhead Line By Phase	186	187	0.046	0.017	130	FALSE	
Overhead Line By Phase	187	188	0.052	0.02	130	FALSE	
Overhead Line By Phase	188	189	0.101	0.056	130	FALSE	
Overhead Line By Phase	188	190	0.034	0.021	40	TRUE	Close
Overhead Line By Phase	190	191	0.083	0.052	190	FALSE	
Overhead Line By Phase	191	192	0.026	0.021	190	FALSE	
Overhead Line By Phase	192	193	0.078	0.064	190	FALSE	
Overhead Line By Phase	193	194	0.066	0.054	190	FALSE	
Overhead Line By Phase	191	195	0.049	0.04	190	FALSE	
Overhead Line By Phase	195	196	0.059	0.046	198	FALSE	
Overhead Line By Phase	183	197	0.05	0.03	40	TRUE	Close
Overhead Line By Phase	197	198	0.11	0.066	130	FALSE	
Overhead Line By Phase	198	199	0.219	0.115	149	FALSE	
Overhead Line By Phase	198	201	0.107	0.056	149	FALSE	
Overhead Line By Phase	201	202	0.047	0.025	149	FALSE	
Overhead Line By Phase	046	203	0.002	0.001	65	TRUE	Close
Overhead Line By Phase	203	204	0.072	0.043	115	FALSE	
Overhead Line By Phase	204	205	0.059	0.033	115	FALSE	

Overhead Line By Phase	205	206	0.152	0.084	115	FALSE	
Overhead Line By Phase	206	207	0.097	0.058	130	FALSE	
Overhead Line By Phase	207	208	0.084	0.05	130	FALSE	
Overhead Line By Phase	208	209	0.021	0.018	198	FALSE	
Cable	209	211	0.109	0.026	20	TRUE	Close
Overhead Line By Phase	048	212	0.002	0.001	80	TRUE	Close
Overhead Line By Phase	212	213	0.094	0.035	130	FALSE	
Overhead Line By Phase	213	214	0.064	0.024	130	FALSE	
Overhead Line By Phase	214	215	0.044	0.017	130	FALSE	
Overhead Line By Phase	215	216	0.001	0.001	198	TRUE	Close
Overhead Line By Phase	216	217	0.064	0.05	198	FALSE	
Overhead Line By Phase	217	218	0.123	0.096	198	FALSE	
Overhead Line By Phase	218	219	0.097	0.076	198	FALSE	
Cable	214	222	0.019	0.005	25	TRUE	Close
Overhead Line By Phase	049	236	0.053	0.028	65	TRUE	Close
Overhead Line By Phase	236	237	0.001	0.001	20	TRUE	Close
Overhead Line By Phase	237	238	0.059	0.035	198	FALSE	
Overhead Line By Phase	238	239	0.027	0.016	198	FALSE	
Overhead Line By Phase	239	240	0.03	0.017	198	FALSE	
Overhead Line By Phase	240	241	0.042	0.024	198	FALSE	
Overhead Line By Phase	050	242	0.024	0.019	100	TRUE	Close
Overhead Line By Phase	242	243	0.005	0.004	260	FALSE	
Overhead Line By Phase	243	244	0.028	0.022	260	FALSE	
Overhead Line By Phase	244	245	0.035	0.028	260	FALSE	
Overhead Line By Phase	245	246	0.012	0.01	260	FALSE	
Overhead Line By Phase	246	247	0.014	0.011	260	FALSE	
Cable	242	248	0.061	0.015	65	TRUE	Close
Cable	248	249	0.012	0.003	267	TRUE	Close

Overhead Line By Phase	244	250	0.023	0.019	198	FALSE	
Cable	250	251	0.021	0.005	65	TRUE	Close
Cable	251	252	0.057	0.014	267	TRUE	Close
Cable	246	253	0.055	0.013	50	TRUE	Close
Cable	246	254	0.057	0.014	50	TRUE	Close
Cable	254	255	0.008	0.002	267	TRUE	Close
Overhead Line By Phase	247	256	0.071	0.057	50	TRUE	Close
Overhead Line By Phase	256	257	0.04	0.032	198	FALSE	
Overhead Line By Phase	052	259	0.028	0.022	198	FALSE	
Cable	259	260	0.079	0.019	80	TRUE	Close
Cable	260	261	0.044	0.011	267	TRUE	Close
Overhead Line By Phase	053	262	0.032	0.026	80	TRUE	Close
Cable	262	263	0.038	0.009	267	TRUE	Close
Cable	263	264	0.041	0.01	267	TRUE	Close
Cable	261	265	0.064	0.015	267	TRUE	Close
Overhead Line By Phase	053	266	0.009	0.007	260	FALSE	
Overhead Line By Phase	266	267	0.026	0.022	80	TRUE	Close
Overhead Line By Phase	267	268	0.076	0.062	190	FALSE	
Overhead Line By Phase	268	269	0.117	0.096	190	FALSE	
Overhead Line By Phase	269	270	0.049	0.04	190	FALSE	
Overhead Line By Phase	270	271	0.045	0.037	190	FALSE	
Overhead Line By Phase	055	272	0.049	0.026	65	TRUE	Close
Overhead Line By Phase	272	273	0.073	0.039	198	FALSE	
Overhead Line By Phase	273	274	0.047	0.025	198	FALSE	
Overhead Line By Phase	274	275	0.039	0.021	198	FALSE	
Overhead Line By Phase	275	276	0.018	0.01	198	FALSE	
Overhead Line By Phase	272	277	0.039	0.021	198	FALSE	
Overhead Line By Phase	276	279	0.023	0.018	20	TRUE	Close
Overhead Line By Phase	057	280	0.005	0.013	20	TRUE	Close
Overhead Line By Phase	280	281	0.034	0.018	198	FALSE	
Overhead Line By Phase	058	282	0.028	0.03	80	TRUE	Close

Overhead Line By Phase	282	283	0.045	0.049	231	FALSE	
Overhead Line By Phase	283	284	0.027	0.029	231	FALSE	
Cable	284	285	0.043	0.011	25	TRUE	Close
Overhead Line By Phase	059	286	0.077	0.06	80	TRUE	Close
Overhead Line By Phase	286	287	0.054	0.042	198	FALSE	
Overhead Line By Phase	287	288	0.067	0.052	198	FALSE	
Overhead Line By Phase	288	289	0.086	0.067	198	FALSE	
Overhead Line By Phase	289	290	0.03	0.023	198	FALSE	
Overhead Line By Phase	288	291	0.13	0.105	198	FALSE	

Child Node Function:	DER 038 (MAIN FEED)	DER 041 (CKT TIE1)	DER 060 (CKT TIE2)	DER 181 (DER1)	DER 247 (DER2)	DER 276 (DER3)
	039	038	038	038	038	038
	040	039	039	039	039	039
	041	040	040	040	040	040
	042	042	041	041	041	041
	043	043	042	042	042	042
	044	044	043	043	043	043
	045	045	044	044	044	044
	046	046	045	046	045	045
	047	047	046	047	046	046
	048	048	047	048	047	047
	049	049	048	049	048	048
	050	050	049	050	049	049
	051	051	050	051	051	050
	052	052	051	052	052	051
	053	053	052	053	053	052
	054	054	053	054	054	053
	055	055	054	055	055	054
	056	056	055	056	056	056
	057	057	056	057	057	057
	058	058	057	058	058	058
	059	059	058	059	059	059
	060	060	059	060	060	060
	172	172	172	172	172	172
	173	173	173	173	173	173
	174	174	174	174	174	174
	175	175	175	175	175	175
	176	176	176	176	176	176
	177	177	177	177	177	177
	178	178	178	178	178	178
	179	179	179	179	179	179
	180	180	180	180	180	180

181	181	181	045	181	181
182	182	182	182	182	182
183	183	183	183	183	183
184	184	184	184	184	184
185	185	185	185	185	185
186	186	186	186	186	186
187	187	187	187	187	187
188	188	188	188	188	188
189	189	189	189	189	189
190	190	190	190	190	190
191	191	191	191	191	191
192	192	192	192	192	192
193	193	193	193	193	193
194	194	194	194	194	194
195	195	195	195	195	195
196	196	196	196	196	196
197	197	197	197	197	197
198	198	198	198	198	198
199	199	199	199	199	199
201	201	201	201	201	201
202	202	202	202	202	202
203	203	203	203	203	203
204	204	204	204	204	204
205	205	205	205	205	205
206	206	206	206	206	206
207	207	207	207	207	207
208	208	208	208	208	208
209	209	209	209	209	209
211	211	211	211	211	211
212	212	212	212	212	212
213	213	213	213	213	213
214	214	214	214	214	214
215	215	215	215	215	215
216	216	216	216	216	216
217	217	217	217	217	217
218	218	218	218	218	218
219	219	219	219	219	219
222	222	222	222	222	222
236	236	236	236	236	236
237	237	237	237	237	237
238	238	238	238	238	238
239	239	239	239	239	239
240	240	240	240	240	240
241	241	241	241	241	241
242	242	242	242	050	242
243	243	243	243	242	243
244	244	244	244	243	244
245	245	245	245	244	245
246	246	246	246	245	246
247	247	247	247	246	247
248	248	248	248	248	248

249	249	249	249	249	249
250	250	250	250	250	250
251	251	251	251	251	251
252	252	252	252	252	252
253	253	253	253	253	253
254	254	254	254	254	254
255	255	255	255	255	255
256	256	256	256	256	256
257	257	257	257	257	257
259	259	259	259	259	259
260	260	260	260	260	260
261	261	261	261	261	261
262	262	262	262	262	262
263	263	263	263	263	263
264	264	264	264	264	264
265	265	265	265	265	265
266	266	266	266	266	266
267	267	267	267	267	267
268	268	268	268	268	268
269	269	269	269	269	269
270	270	270	270	270	270
271	271	271	271	271	271
272	272	272	272	272	055
273	273	273	273	273	272
274	274	274	274	274	273
275	275	275	275	275	274
276	276	276	276	276	275
277	277	277	277	277	277
279	279	279	279	279	279
280	280	280	280	280	280
281	281	281	281	281	281
282	282	282	282	282	282
283	283	283	283	283	283
284	284	284	284	284	284
285	285	285	285	285	285
286	286	286	286	286	286
287	287	287	287	287	287
288	288	288	288	288	288
289	289	289	289	289	289
290	290	290	290	290	290
291	291	291	291	291	291

Results

Connected Nodes	Micro-grid 1 Loads Served	Loads Not Served
'038'	'039'	
'039'	'172'	
'040'		

'172'

Connected Nodes	Micro-grid 2 Loads Served	Loads Not Served
'041'	'043'	
'042'	'174'	
'043'	'175'	
'044'	'176'	
'173'	'177'	
'174'	'179'	
'175'	'180'	
'176'		
'177'		
'178'		
'179'		
'180'		

Connected Nodes	Micro-grid 3 Loads Served	Loads Not Served
'052'	'053'	
'053'	'054'	
'054'	'058'	
'055'	'260'	
'056'	'261'	
'057'	'263'	
'058'	'264'	
'059'	'265'	
'060'	'266'	
'259'	'268'	
'260'	'269'	
'261'	'270'	
'262'	'271'	
'263'	'281'	
'264'	'282'	
'265'	'283'	
'266'	'285'	
'267'	'286'	
'268'	'287'	
'269'	'288'	
'270'	'289'	

'271'	'290'
'280'	'291'
'281'	
'282'	
'283'	
'284'	
'285'	
'286'	
'287'	
'288'	
'289'	
'290'	
'291'	

Connected Nodes	Micro-grid 4 Loads Served	Loads Not Served
'045'	'051'	'187'
'046'	'181'	'196'
'047'	'182'	'201'
'048'	'184'	'205'
'049'	'185'	'206'
'050'	'186'	
'051'	'189'	
'181'	'191'	
'182'	'192'	
'183'	'193'	
'184'	'194'	
'185'	'195'	
'186'	'198'	
'187'	'199'	
'188'	'202'	
'189'	'204'	
'190'	'207'	
'191'	'208'	
'192'	'211'	
'193'	'213'	
'194'	'215'	
'195'	'217'	
'196'	'218'	
'197'	'219'	
'198'	'222'	

'199'	'236'
'201'	'238'
'202'	'239'
'203'	'240'
'204'	'241'
'205'	
'206'	
'207'	
'208'	
'209'	
'211'	
'212'	
'213'	
'214'	
'215'	
'216'	
'217'	
'218'	
'219'	
'222'	
'236'	
'237'	
'238'	
'239'	
'240'	
'241'	

Connected Nodes	Micro-grid 5 Loads Served	Loads Not Served
'242'	'243'	'245'
'243'	'244'	
'244'	'248'	
'245'	'249'	
'246'	'251'	
'247'	'252'	
'248'	'253'	
'249'	'254'	
'250'	'255'	
'251'	'256'	
'252'	'257'	
'253'		

'254'
'255'
'256'
'257'

Connected Nodes	Micro-grid 6 Loads Served	Loads Not Served
'272'	'272'	
'273'	'274'	
'274'	'275'	
'275'	'276'	
'276'	'277'	
'277'	'279'	
'279'		